Regular Article

Phase and precession evolution in the Burgers equation[⋆]

Michele Buzzicotti[1], Brendan P. Murray[2], Luca Biferale[1], and Miguel D. Bustamante[2,a]

[1] Department of Physics and INFN, University of Rome "Tor Vergata", Via della Ricerca Scientifica 1, 00133, Rome, Italy
[2] Complex and Adaptive Systems Laboratory, School of Mathematics and Statistics, University College Dublin, Belfield, Dublin 4, Ireland

Abstract. We present a phenomenological study of the phase dynamics of the one-dimensional stochastically forced Burgers equation, and of the same equation under a Fourier mode reduction on a fractal set. We study the connection between coherent structures in real space and the evolution of triads in Fourier space. Concerning the one-dimensional case, we find that triad phases show alignments and synchronisations that favour energy fluxes towards small scales —a direct cascade. In addition, strongly dissipative real-space structures are associated with entangled correlations amongst the phase precession frequencies and the amplitude evolution of Fourier triads. As a result, triad precession frequencies show a non-Gaussian distribution with multiple peaks and fat tails, and there is a significant correlation between triad precession frequencies and amplitude growth. Links with dynamical systems approach are briefly discussed, such as the role of unstable critical points in state space. On the other hand, by reducing the fractal dimension D of the underlying Fourier set, we observe: i) a tendency toward a more Gaussian statistics, ii) a loss of alignment of triad phases leading to a depletion of the energy flux, and iii) the simultaneous reduction of the correlation between the growth of Fourier mode amplitudes and the precession frequencies of triad phases.

1 Introduction

The physics of extended nonlinear dynamical systems is often characterised by fluctuations at different frequencies and/or wavelengths. In many cases it is key to disentangle the evolution of amplitudes and phases of such fluctuations [1–3]. In this paper we consider the context of nonlinear partial differential equations (PDEs) describing the interaction of oscillating Fourier modes (waves) with quadratic nonlinearities in general, and the application to the one-dimensional Burgers equation:

$$\frac{\partial u}{\partial t} + \frac{1}{2}\frac{\partial u^2}{\partial x} = \nu \frac{\partial^2 u}{\partial x^2} + f, \qquad (1)$$

where $u(x,t)$ is the space periodic velocity, ν is a positive parameter (viscosity) and $f(x,t)$ is the external forcing. The Burgers equation, see [4] for a review, is a model for various nonlinear dissipative systems. It describes a variety of nonlinear wave phenomena such as acoustic waves and plasma physics [5]. When driven by a random forcing it has applications in condensed matter problems like

interface deposition and growth (see for instance [6]). In the absence of a driving force, the explicit solution provided by the Hopf-Cole method [7,8] leads to non-trivial problems in the limit of vanishing viscosity, when random initial conditions are assumed. This is particularly important for the evolution of large-scale structures in the Universe [9–13]. Burgers equation was originally conceived as a toy model for turbulence and it is frequently used as a testing ground for numerical schemes and as a training ground for developing mathematical tools to study Navier-Stokes turbulence and other hydrodynamical or Lagrangian problems [14–19].

Burgers equation represents one of the simplest nonlinear partial differential equations known to display a non-trivial scaling of the velocity field correlation functions. Multiscaling is connected to the tendency to create shocks and consequently to increase negative velocity differences $\Delta_r u < 0$ and decrease positive ones $\Delta_r u > 0$, where $\Delta_r u = u(x+r,t) - u(x,t)$. Thus a strongly non-Gaussian probability distribution function (PDF) of $\Delta_r u$ is observed. The presence of strongly localised velocity jumps (shocks) in the real space is the fingerprint of Burgers's dynamics. We remark that shocks are the only structures in the flow able to dissipate energy in the limit of small viscosity. In other words, the energy flux across scales is absorbed only by a few strongly localised events

---

[⋆] Contribution to the Topical Issue "Multi-scale phenomena in complex flows and flowing matter" edited by Luca Biferale, Massimo Cencini, Alessandra Lanotte and Mauro Sbragaglia.

[a] e-mail: `miguel.bustamante@ucd.ie`

in real space. The guiding motivation of this paper is to look for relations between the real-space multiscaling properties and the Fourier dynamics, a key problem also in Navier-Stokes turbulence [20,21].

We will work almost exclusively with Fourier mode variables $\hat{u}_k(t)$ rather than the real periodic field $u(x,t)$, where $u(x,t) = \sum_{k\in\mathbb{Z}} e^{ikx}\hat{u}_k(t)$ with x the position in real space and k the wave numbers. Reality of $u(x,t)$ implies $\hat{u}_{-k}(t) = \hat{u}_k^*(t)$, where * denotes complex conjugation. When Galerkin truncations are considered, the range for the sum above is reduced: instead of summing over $k \in \mathbb{Z}$ we sum over a given subset: $k \in \mathcal{C}$, where $\mathcal{C} \subset \mathbb{Z}$. Each mode is indexed by an integer wave number k. The dynamical content of mode k is given by its complex valued Fourier amplitude, $\hat{u}_k(t)$. Using this representation, the governing PDE can be decomposed into a set of ordinary differential equations (ODEs) which describe the individual evolution of each of the complex amplitudes. To further separate the variables of interest, an amplitude/phase representation will be used: $\hat{u}_k(t) = a_k(t)e^{i\phi_k(t)}$, where $a_k(t) = |\hat{u}_k(t)|$ (amplitude) and $\phi_k(t) = \arg[\hat{u}_k(t)]$ (phase).

In Burgers equations the nonlinearity is quadratic so interactions appear in *triads* (groups of 3 modes). The *key* dynamical degrees of freedom consist of the modes' real amplitudes $a_k(t)$ along with the *triad phases*, i.e. the combinations:

$$\varphi_{k_1,\,k_2}^{k_3}(t) = \phi_{k_1}(t) + \phi_{k_2}(t) - \phi_{k_3}(t),$$

where the wave numbers k_1, k_2, k_3 satisfy a "closed-triad" condition: $k_1 + k_2 = k_3$. By simple counting, one obtains that many triad phases are not linearly independent; a maximal set of linearly independent triad phases is easily found once the set of wave numbers $\mathcal{C}$ is known. From here on, we will call "state space" the collection of modes' real amplitudes along with a maximal set of linearly independent triad phases.

The motivation for studying the evolution of these key dynamical degrees of freedom is that they provide quantitative information about the energy exchanges taking place in the system. For example, it was shown in [22] for the 2D barotropic vorticity equation with periodic boundary conditions that the triad phases $\varphi_{k_1,\,k_2}^{k_3}(t)$ not only oscillate in time but also *precess* (or drift). This precession gives rise to a new frequency, the so-called precession frequency, which is approximately equal to the value of the zero-mode in time of $\dot{\varphi}_{k_1,\,k_2}^{k_3}(t)$. When the precession frequency of a given triad is equal to zero or coincides with a typical frequency of the system's oscillation, then there is a *precession resonance*, characterised by strong energy transfers. To see how this works, the contribution from a given triad to the energy flux towards small scales (to be defined below in sect. 2) is proportional to the time/ensemble average $\langle a_{k_1}a_{k_2}a_{k_3}\sin(\varphi_{k_1,\,k_2}^{k_3})\rangle$. Two resonant scenarios are possible regarding the phase behaviour. i) The triad phase simply oscillates near the value $\pi/2$ mod 2π. We get a non-zero contribution to the energy transfer from this average because $a_{k_1}a_{k_2}a_{k_3} > 0$

by definition. This corresponds to precession resonance with zero precession frequency: $\langle\dot{\varphi}_{k_1,\,k_2}^{k_3}\rangle \approx 0$. ii) The phase drifts with non-zero precession frequency, for example $\varphi_{k_1,\,k_2}^{k_3}(t) \approx \Omega\,t$. Thus, the contribution to the flux has the form $\langle a_{k_1}a_{k_2}a_{k_3}\sin(\Omega\,t)\rangle$, which will not vanish if Ω coincides with a typical frequency of the time signal of $a_{k_1}a_{k_2}a_{k_3}$. This corresponds to precession resonance with non-zero precession frequency: $\langle\dot{\varphi}_{k_1,\,k_2}^{k_3}\rangle \approx \Omega \neq 0$. Both resonant scenarios can involve multiple triads in synchrony, resulting in strong energy transfers across multiple scales of the system. This phenomenon leads naturally to the study of invariant manifolds within the state space. In [22], precession resonances were shown to correspond dynamically to trajectories embedded in the unstable manifolds of periodic orbits. These unstable manifolds have components that extend towards large values of amplitudes, $a_k(t)$, contributing directly to intense energy-transfer events.

The aim of this study is twofold. First, we want to study the relevance of triad phases and their precession frequencies relating to the energy transfers amongst modes, focusing on: i) Probability distribution of triad phases, joint probability distributions between different triad phases and probability distribution of triad phase precession frequencies. ii) Joint probability distributions between precession frequencies and energy content and also between precession frequencies and growth rate of energy transfers. Second, in order to better understand the connections between these statistical properties and the presence of shock-like structure in the real space, we will study the effect of the introduction of a quenched disorder given by the projection of the dynamics on a fractal Fourier set, where preliminary results show a strong depletion of shocks [23] with reduced system fractal dimension. We will complement these studies with dynamical-system interpretations in terms of correlations and synchronisation within the state space.

2 Burgers equation in one dimension and less

Let us start from eq. (1) written in Fourier space:

$$\frac{\partial\hat{u}_k}{\partial t} = -\frac{ik}{2}\sum_{k_1}\hat{u}_{k_1}\hat{u}_{k-k_1} - \nu k^2\hat{u}_k + \hat{f}_k, \qquad (2)$$

where energy is dissipated from the viscous term and injected by the external forcing. The core of the dynamics is in the quadratic nonlinear convolution, a term that globally conserves energy by redistributing it amongst Fourier modes. Let us define the stationary Energy spectrum as

$$\langle\hat{u}_k\hat{u}_{k'}\rangle = E_k\delta(k+k'), \qquad (3)$$

where $\langle\bullet\rangle$ denotes an average over the statistically steady ensemble. The energy flux in the positive direction across a wave number k is defined as $\Pi(k) \equiv -\frac{\mathrm{d}}{\mathrm{d}t}(\sum_{k_1=0}^{k}E_{k_1})$. From (2) and (3) it is easy to realise that the contribution
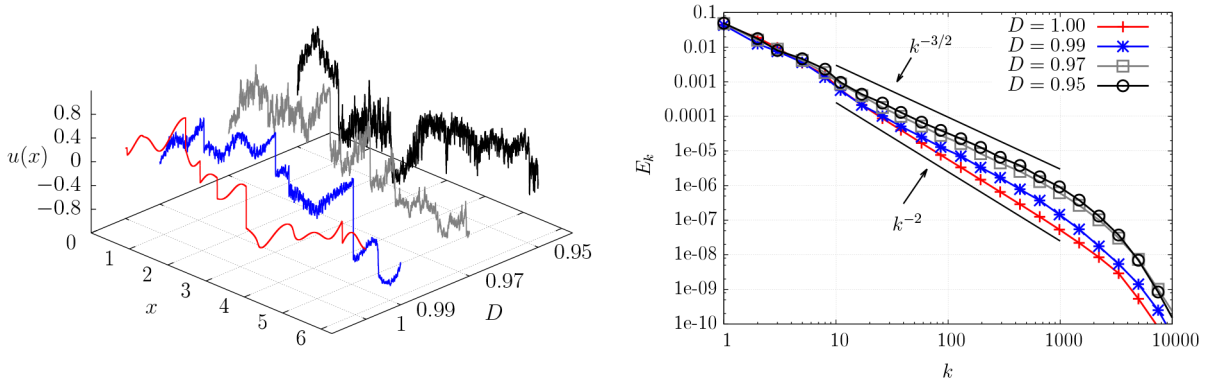
Fig. 1. Left: Snapshots of real space velocity profiles as a function of space and fractal Fourier dimension: $D = 1$ (red), $D = 0.99$ (blue), $D = 0.97$ (grey) and $D = 0.95$ (black). Right: Mean energy spectra in log-log scale, obtained for the same four fractal dimensions D and using the same colour code as in the left panel. The black solid line is the scaling slope k^{-2} produced by the undecimated ($D = 1.0$) Burgers equation.

from the nonlinear interactions to this energy flux is given by the "triadic terms"

$$\Pi(k) = \sum_{k_1=1}^{k} \sum_{k_2=-\infty}^{\infty} k_1 \, \Im \left\{ \langle \hat{u}_{k_1} \hat{u}_{k_2} \hat{u}_{k_1+k_2}^* \rangle \right\}, \quad (4)$$

where $\Im\{z\}$ denotes the imaginary part of z. It is important to point out that the energy exchange produced by the nonlinear term inside a single triad is conservative. Indeed, the sum of the energy variation at three wave numbers with $k_1 + k_2 = k_3$ is always zero. This implies that the energy flux across a scale k is only given by the energy exchanges inside triads which have at least one wave number higher than k and one smaller than k. Hence, $\Pi(\infty)$ is always equal to zero [24–27]. In particular, at those scales where neither the forcing mechanism nor the viscous term play any relevant role, the dynamics are fully dominated by the nonlinear evolution, the so-called "inertial-range" of scales. For smaller and smaller viscosity, the solution of Burgers equations develops a velocity configuration with sharper and sharper shock-like structures (see fig. 1), characterised by a power-law spectrum $E(k) \propto k^{-2}$ (see [4]).

2.1 Phases and fluxes

Focusing on the nonlinear term of the Burgers equation (11) and making the following substitution

$$\hat{u}_k(t) = a_k(t) e^{i\phi_k(t)}, \qquad a_k(t) \equiv |\hat{u}_k(t)|, \quad (5)$$

and recalling the definition of triad phase

$$\varphi_{k_1,k_2}^{k_3}(t) = \phi_{k_1}(t) + \phi_{k_2}(t) - \phi_{k_3}(t), \quad (6)$$

we get the evolution for the amplitude a_k and phase ϕ_k of the surviving modes:

$$\dot{a}_k = \frac{k}{2} \theta_k \sum_{k_1,k_2} a_{k_1} a_{k_2} \, \theta_{k_1} \theta_{k_2} \sin(\varphi_{k_1,k_2}^{k}) \, \delta_{k_1+k_2,k}, \quad (7)$$

$$\dot{\phi}_k = -\frac{k}{2} \theta_k \sum_{k_1,k_2} \frac{a_{k_1} a_{k_2}}{a_k} \, \theta_{k_1} \theta_{k_2} \cos(\varphi_{k_1,k_2}^{k}) \, \delta_{k_1+k_2,k}. \quad (8)$$

Note that the factor θ_k in the latter equations is the projector in front of the nonlinear term in eq. (11), while θ_{k_1} and θ_{k_2} represent the fact that also the other two modes satisfying the triadic condition are decimated.

It is evident from eqs. (6), (7) and (8) that $\varphi_{k_1,k_2}^{k_3}$, along with a_k, satisfy a closed system of equations which determines the nonlinear dynamics. In particular, the individual phases ϕ_k can be obtained by quadratures from eq. (8).

Applying substitutions (5)–(6) to the velocity field in the energy flux equation, eq. (4), we get

$$\Pi(k) = \sum_{k_1=1}^{k} \sum_{k_2=-\infty}^{\infty} \left\langle a_{k_1} a_{k_2} a_{k_1+k_2} \sin(\varphi_{k_1,k_2}^{k_1+k_2}) \right\rangle$$
$$\times k_1 \theta_{k_1} \theta_{k_2} \theta_{k_1+k_2}. \quad (9)$$

As expected, the energy flux depends on the phases via $\varphi_{k_1,k_2}^{k_1+k_2}$ only. The crucial observation is that the sign of the contributions to this energy flux depends only on the values of the triad phases, because all other factors appearing in (9) are positive, including the real amplitudes a_k. Since the sign of the energy flux determines the cascade direction, it is very important to analyse these contributions in detail.

Define k_3 by the triad relation $k_1 + k_2 = k_3$. Following an analogous method to the detailed energy balance of triads [24–27], we deduce that non-zero contributions to the energy flux (9) come from triads that have at least 1 mode within the interval $[-k, k]$ and at least 1 mode outside it. Combining these contributions we obtain

$$\Pi(k) = \sum_{k_1=1}^{k} \sum_{k_3=k+1}^{\infty} 2k_1 \left\langle a_{k_1} a_{k_2} a_{k_3} \sin(\varphi_{k_1,k_2}^{k_3}) \right\rangle,$$

where we have used the reality of the original field, which implies $\phi_{-k_j} = -\phi_{k_j}$ and $a_{-k_j} = a_{k_j}$. We remark the wave number ordering: $0 < k_1 < k_3$, $0 < k_2 < k_3$ and $k_3 = k_1 + k_2$.

In summary, the sign of each individual triad's contribution depends solely on the sign of $\sin(\varphi_{k_1,k_2}^{k_3})$, where

k_1, k_2, k_3 is the "ordered" version of that triad, with $k_3 = k_1 + k_2$ and $k_j > 0$. As a result, when $\varphi_{k_1,k_2}^{k_3}$ is close to $\frac{\pi}{2} + 2n\pi$, $n \in \mathbb{Z}$, the direct-cascade energy flux is maximised (at fixed amplitudes). In sect. 3.1 we present statistical analyses that show that triad phases tend to cluster near these values, involving in addition a synchronisation amongst different triads, so that several terms contribute with a positive sign, leading to direct-cascade flux whose intensity depends on the dimension of the Fourier fractal set where modes live.

2.2 Burgers equation on fractal Fourier sets

In order to study the effects of the quenched noise on the triadic interactions in Fourier space, we use a projection method to fractal sets. This projection method was originally introduced in [28] to study the inverse energy cascade in 2D Navier-Stokes equations (see [29] for a review). Later, it was exploited to study the statistical properties of small-scale fluctuations in the 3D Navier-Stokes equations [30] and 1D Burgers equation [23]. In these two papers, a tendency towards more regular Gaussian statistics for the small-scale velocity field was observed at lower values of fractal dimension D, indicating that the disorder leads to an energy transfer regime characterised by self-similar fluctuations.

The projection on a fractal Fourier set is done using a decimation operator P_D acting on the field $u(x,t)$ as

$$v(x,t) = P_D u(x,t) = \sum_k e^{ikx} \theta_k \hat{u}_k(t). \qquad (10)$$

Here θ_k, $k \in \mathbb{N}$ are independently chosen random numbers such that $\theta_k = 1$, with probability h_k and $\theta_k = 0$, with probability $1-h_k$. We also impose the condition that $\theta_k = \theta_{-k}$ to ensure the reality of the field at all times. Choosing $h_k = k^{D-1}$, with $0 < D \leq 1$, we introduce a quenched disorder which randomly suppresses modes on the Fourier lattice and ensures that on average we have $N(k) \propto k^D$ surviving modes inside an interval of length k around the origin. Applying this projector to the Burgers equation, we can then write the decimated PDE as

$$\frac{\partial v}{\partial t} + \frac{1}{2} P_D \frac{\partial v^2}{\partial x} = \nu \frac{\partial^2 v}{\partial x^2} + P_D f. \qquad (11)$$

We performed a set of numerical simulations of eq. (11) by changing the dimension between $D = 1$ and $D = 0.95$. We chose the forcing to be Gaussian and white-in-time

$$\langle \hat{f}(k_1, t_1) \hat{f}(k_2, t_2) \rangle = 2f_0 |k_f|^{-1} \delta(t_1 - t_2) \delta(k_1 + k_2), \qquad (12)$$

acting only at large scales, the forced wave numbers k_f are all the non-decimated modes in the range $[1:8]$. For the numerical simulation we used Adams-Bashforth schemes of fourth order, with a number of collocation points ranged between $N = 2^{16}$ and $N = 2^{19}$, and a time step $\delta t \sim 10^{-5}$. See table 1 for more details about the numerical data. Figure 1 shows a snapshot of the velocity field for four different values of fractal dimension D, together with the

Table 1. D: dimension of the Fourier fractal set where modes live. N: number of collocation points. $\%(D)$: percentage of decimated wave numbers, where the first value is related to the lower resolution used while the second value is related to the higher resolution. ν: value of the kinematic viscosity. k_f: forced wave numbers. δt: Numerical time step used in the temporal evolution.

D	N	$\%(D)$	ν	k_f	δt
1	2^{16}–2^{19}	0	$8 \cdot 10^{-5}$	$[1:8]$	$5.5 \cdot 10^{-5}$
0.99	2^{16}–2^{19}	8–10	$2.5 \cdot 10^{-5}$	$[1:8]$	$2.3 \cdot 10^{-5}$
0.97	2^{16}–2^{19}	23–27	$9 \cdot 10^{-6}$	$[1:8]$	$2.0 \cdot 10^{-5}$
0.95	2^{16}–2^{19}	36–40	$5 \cdot 10^{-6}$	$[1:8]$	$1.7 \cdot 10^{-5}$

mean energy spectra. It is important to mention that in fig. 1 the spectra have no gaps because we have further performed an average over different quenched fractal masks [23]. As one can see, shocks are present for all fractal dimensions, while the smooth (for $D = 1$) ramps connecting two shocks develop small-scale fluctuations that become more and more pronounced as the fractal dimension D decreases. It is important to remark that even if the disorder produces a non-trivial change in the spectrum, a power-law behaviour is always present [23]. Similar results have also been observed in the three-dimensional Navier-Stokes equations [30]. A scaling of k^{-2} is recovered in the undecimated $D = 1$ case.

3 Numerical results

3.1 Phase analysis

We present a phenomenological study of Burgers triad phase dynamics. Let us first consider the case when we define all phases in the same periodic range, $\varphi_{k_1,k_2}^{k_3}(t) \in [-\pi, \pi]$, i.e., we omit the phase precessions for the moment. In fig. 2 (left panel) we show the PDF of $\varphi_{k_1,k_2}^{k_3}(t)$ for three different triads composed of wave numbers belonging to the inertial range and ordered in the usual way $0 < k_1 < k_2 < k_3$ with $k_3 = k_1 + k_2$

$$T_1 \rightarrow [k_1; k_2; k_3] = [100; 150; 250],$$
$$T_2 \rightarrow [k_1; k_2; k_3] = [200; 250; 450],$$
$$T_3 \rightarrow [k_1; k_2; k_3] = [300; 350; 650],$$

at $D = 1$ and $D = 0.95$. The undecimated case $D = 1$ shows a more marked preference for triad phase alignments about $\pi/2$, which maximises the energy flux because flux contributions are proportional to $\sin(\varphi_{k_1,k_2}^{k_3})$ (see eq. (9)). The PDFs are peaked at $\pi/2$ and have a minimum at $3\pi/2$, which suggests that the energy flux is, on average, directed from large to small scales. This would be true provided one assumes that real amplitudes a_k take higher or similar values when phases are near $\pi/2$ than when phases are near $3\pi/2$. This assumption is confirmed by simulations, so we have a direct cascade of energy as in
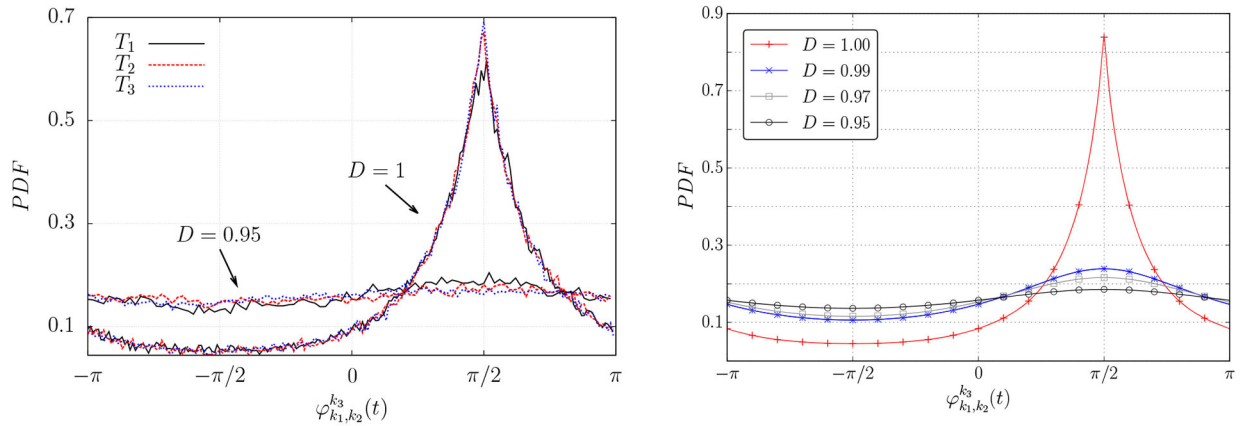
Fig. 2. Left: Histograms of triad phase (mod 2π with offset $-\pi$) computed during the temporal evolution of different triads in the inertial range. $T_1 : [k_1; k_2; k_3] = [100; 150; 250]$ (black solid line), $T_2 : [k_1; k_2; k_3] = [200; 250; 450]$ (red dashed line), and $T_3 : [k_1; k_2; k_3] = [300; 350; 650]$ (blue dotted line). To aid comparison, the undecimated case ($D = 1$) and decimated case ($D = 0.95$) are plotted together. Right: Same type of histograms but over all 160 801 triads composed of wave numbers inside the range $100 \leq k \leq 1000$, and for the same set of values of fractal Fourier dimension D and colour code as in fig. 1.

3D Navier-Stokes turbulence. On the other hand, for the case $D = 0.95$ we no longer have a marked peak at $\pi/2$, especially when we consider the triad T_3 which is the one containing higher wave numbers. This is the first evidence that the introduction of the quenched disorder strongly perturbs the coherence of the energy transfer mechanism, leading to a much slower direct cascade. In fig. 2 (right panel) we show a similar study but this time involving over 160 thousand triads with wave numbers in the range $[100, 1000]$. The features just discussed for the selected triads are again there, which shows that most triads are behaving in basically the same way.

A qualitative view of the correlation amongst different triad phases throughout the system's evolution is proposed in fig. 3. Here a scatter plot between the phase of triads T_1 and T_2 is shown, where the phase angle is not constrained to be on a periodic domain. From the left panel (undecimated Burgers equations $D = 1$) it is clear that a correlation is present between the two phases. A lattice-like distribution with the presence of many clusters indicates that for long periods the two phases are oscillating around a fixed value before jumping simultaneously toward other values. As expected, these clusters exist around values of $\pi/2 + 2n\pi$, $n \in \mathbb{Z}$. This synchronization is directly linked to the results shown in fig. 2 where we saw a peak in the PDF for phase values at $\pi/2$. Since most triad phases spend most of their time near $\pi/2$, it is natural that several triads will be simultaneously near those values for some of the time. In contrast, results for $D = 0.99$ and 0.95 in fig. 3, centre and right panels, show that the synchronization amongst different triad phases is washed out when the quenched disorder is introduced.

Remarkably, synchronisation of triad phases has a direct effect on the energy flux. The more triads are synchronised near $\pi/2 + 2n\pi$, the more positive terms add together to contribute to the flux in eq. (9), leading to a large flux. Thus, loss of synchronisation diminishes the flux via cancellations of positive and negative terms.

3.2 Precession analysis

The "drift" or "precession" of triad phases made evident from fig. 3 suggests that we study the distribution of precession frequencies of the various triad phases in the system, as this distribution can have an impact on the energy fluxes via precession resonance [22]. In order to analyse the phase-precession statistical and dynamical properties, it is important to filter out the high-frequency fluctuations introduced by the evolution of each of the phase variables contributing to the triad phase. Therefore, let us define the triad phase precession averaged on a time window Δt as

$$\Omega_{k_1 k_2}^{k_3}(t, \Delta t) \equiv \frac{1}{N} \sum_{t_i = t}^{t + \Delta t} \dot{\varphi}_{k_1 k_2}^{k_3}(t_i), \qquad (13)$$

where t_i denote data points from the numerical integration and the time window, $\Delta t = N \delta t$, where δt is the numerical time step and N is a large enough integer to remove the noise at the dissipative scales. But Δt should be chosen small enough not to kill all temporal correlations in the system. In practice we choose Δt of the order of the Kolmogorov time microscale $t_\eta \equiv \sqrt{\frac{\nu}{\varepsilon}} \approx 10^{-2}$. The instantaneous phase precession, $\dot{\varphi}_{k_1 k_2}^{k_3}(t)$, is defined in terms of the finite-difference increments of individual phase derivatives $\dot{\phi}_k(t)$:

$$\dot{\phi}_k(t_i) = \frac{\phi_k(t_i + \delta t) - \phi_k(t_i)}{\delta t} = \frac{1}{\delta t} \arg \left[\frac{\hat{u}_k(t_i + \delta t)}{\hat{u}_k(t_i)} \right]. \qquad (14)$$

The probability density functions (PDFs) of $\Omega_{k_1 k_2}^{k_3}(t, \Delta t)$ are produced by considering all 160 801 triads constructed from modes inside an interval in the inertial range: $k \in I_k = [100, 1000]$. In fig. 4 we show the corresponding PDFs for three different time windows: $\Delta t = 1000 \, \delta t = 0.5 \, t_\eta$ (top row); $\Delta t = 2000 \, \delta t = 1.0 \, t_\eta$ (middle row); $\Delta t = 6000 \, \delta t = 3.0 \, t_\eta$ (bottom row). Furthermore,
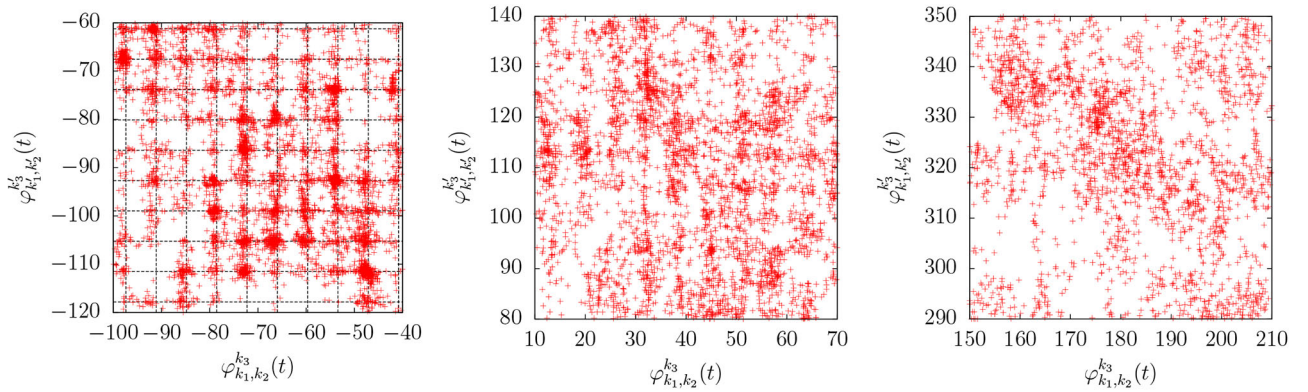
Fig. 3. Parametric plots of the phase evolution for two different triads in the inertial range: $T_1 : [k_1; k_2; k_3] = [100; 150; 250]$ and $T_2 : [k_1; k_2; k_3] = [200; 250; 450]$, showing synchronisation events near $\frac{\pi}{2} + 2n\pi$, $n \in \mathbb{Z}$. Left: Fractal Fourier dimension $D = 1$. Grid lines denote triad phase values at $\frac{\pi}{2} + 2n\pi$. Centre: Fractal Fourier dimension $D = 0.99$. Right: Fractal Fourier dimension $D = 0.95$.

we also compare the results obtained from the original undecimated ($D = 1$) Burgers equation (left), with two different decimated systems: $D = 0.99$ (centre) and $D = 0.95$ (right). We first note the appearance of secondary peaks in the PDFs, corresponding to non-zero precession frequency values. The number of peaks increases as the time window Δt increases because the triad phase has had enough time to make several jumps between adjacent trapping regions, namely from $\pi/2 + 2n\pi$ to $\pi/2 + 2n'\pi$, with $|n - n'| = 1$, in apparently random sequences (figure not shown, but the jumpy behaviour is evident from the scatter plots of fig. 3). Similarly, the peaks become more pronounced as Δt increases because the longer averaging window leads to a suppression of oscillations in $\varphi_{k_1 k_2}^{k_3}$ around the trapping regions $\pi/2 + 2n\pi$. This explanation also applies to the secondary peaks where the time window Δt includes both the oscillations of $\varphi_{k_1 k_2}^{k_3}$ referred to above but also a number of jumps in $\varphi_{k_1 k_2}^{k_3}$ towards other trapping regions. As Δt is increased the contributions of the oscillations are suppressed but the contributions from the jumps will accumulate. The second interesting feature is the sudden disappearance of the secondary precession-frequency peaks as we decimate the system. At $D = 0.99$ they are barely detectable and at $D = 0.95$ they have been wiped out. This is in line with the results presented in figs. 2 and 3, showing a transition from a structured phase evolution for $D = 1$ to a disordered distribution when decimation is applied.

In order to explore the energy flux it is also important to examine the correlation between evolution of triad precession and triad amplitude. For the same subset of triads, $k_1 + k_2 = k_3$ in the range I_k, we computed two different joint PDFs, corresponding to the correlation amongst the triad precession $\Omega_{k_1 k_2}^{k_3}(t, \Delta t)$ and the temporal average, over Δt, of: i) the modulus of the product of the mode amplitudes,

$$\langle |a_{k_1} a_{k_2} a_{k_3}| \rangle_{\Delta t}, \tag{15}$$

and ii) the modulus of the product of the logarithmic time derivatives of the mode amplitudes,

$$\left\langle \left| \frac{\dot{a}_{k_1} \dot{a}_{k_2} \dot{a}_{k_3}}{a_{k_1} a_{k_2} a_{k_3}} \right| \right\rangle_{\Delta t}. \tag{16}$$

The motivation for choosing these quantities is that they provide a fair comparison weight, amongst different triads, with respect to energy content i) and flux of energy ii).

In fig. 5 we show the resulting joint PDFs for a time window $\Delta t = 3.0 \, t_\eta$, together with its dependence on the fractal dimension D. From these PDFs one can again detect the presence of secondary correlation peaks in the undecimated case only ($D = 1$). The introduction of the quenched disorder destroys the cross-correlations amongst amplitudes and phase precessions.

A closer inspection of fig. 5 reveals a connection with a dynamical systems approach, which deserves some mention here. By definition, a critical point of system (8) is a point in the state space where *all* time derivatives $\dot{a}_k$ and $\dot{\varphi}_{k_1 k_2}^{k_3}$ are equal to zero simultaneously, for all modes and triads. The most common type of critical point is the so-called "unstable": the state of the system may approach such a point along some directions, getting close to it but eventually separating from it along other directions. Thus, active energy exchanges are expected if the state of the system gets close to an unstable critical point. The evidence from fig. 5 is that the state of the Burgers system visits unstable critical points regularly during the evolution: notice the tail near $\dot{a}_k = 0$, $\dot{\varphi}_{k_1 k_2}^{k_3} = 0$ at the lower part of the bottom left panel. Moreover, this tail is correlated, by definition, with the tail at the upper part of the top left panel, corresponding to events of maximum amplitude, *i.e.*, high energy transfers. Finally, fig. 3 suggests that these critical points are distributed preferentially near values of the triad phases given by $\varphi_{k_1 k_2}^{k_3} = \pi/2 + 2n\pi$. In contrast, in the fractal decimated case ($D = 0.95$; see fig. 5, right panels) the
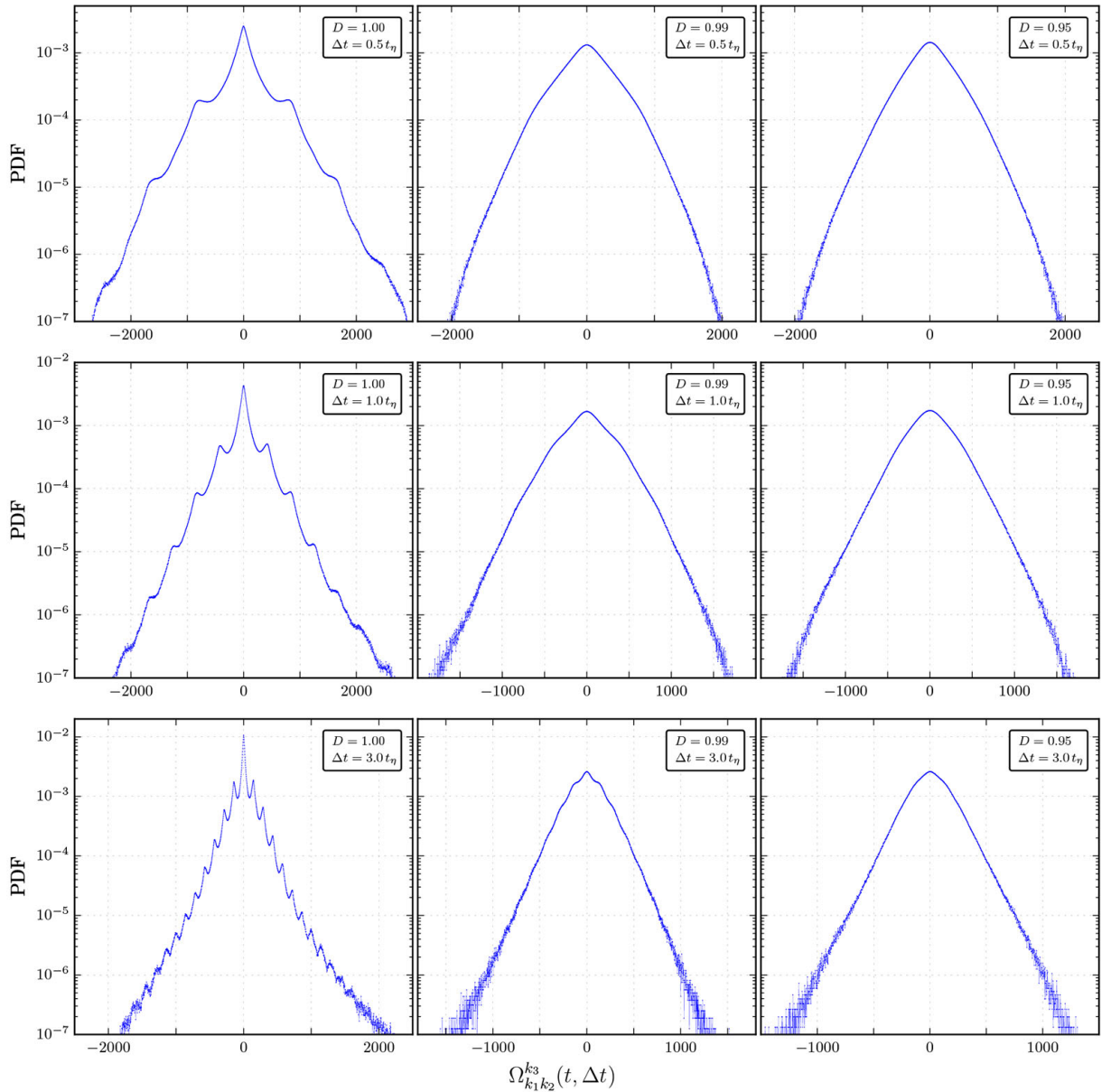
Fig. 4. Probability density functions (PDFs) of the time-averaged triad precessions $\Omega_{k_1 k_2}^{k_3}(t, \Delta t)$ (over time window Δt, see eq. (13)). The PDFs are computed over all 160 801 triads composed of wave numbers inside the range $100 \leq k \leq 1000$ and for the temporal evolution $0 \leq t \leq 10^3 t_\eta$. Top row: $\Delta t = 1000 \, \delta t = 0.5 \, t_\eta$. Middle row: $\Delta t = 2000 \, \delta t = 1.0 t_\eta$. Bottom row: $\Delta t = 6000 \, \delta t = 3.0 \, t_\eta$. The three panels in each row represent different fractal dimensions. Left: $D = 1$. Centre: $D = 0.99$. Right: $D = 0.95$.

above-mentioned tails lose coherence, which could mean that the state visits critical points less often or that less critical points exist. These and other implications will be studied in detail in subsequent work.

4 Conclusions

In this work we have presented numerical results about the evolution of the phases of the triadic structures responsible for the energy transport in the Fourier representation of 1D Burgers equation. Figure 2 shows that the

PDFs of these phases are characterised by marked peaks at $\pi/2 + 2n\pi$, consistent with the presence of a well-defined energy flux directed towards the small scales. In addition, strong correlations between the phase evolution of different triads are presented in fig. 3. These correlations hint to the entangled interactions and synchronisation developed by the Burgers nonlinearity amongst all the Fourier modes in order to provide the well-known energy cascade.

The PDF of precession frequencies, fig. 4, shows a structure of secondary peaks with significant probability, circumscribed by a non-Gaussian (fat-tailed) envelope. This non-trivial feature motivates the search for higher-order
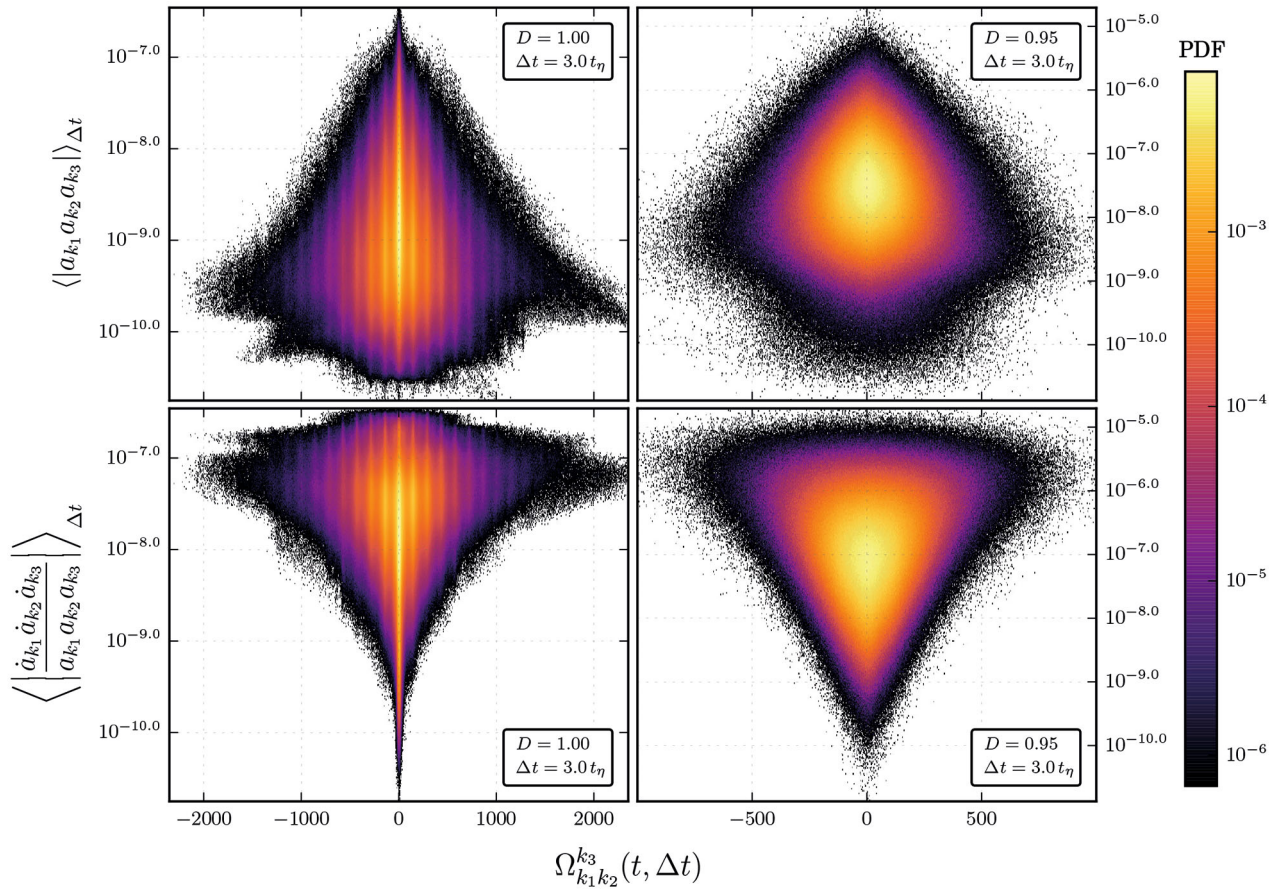
Fig. 5. Joint PDFs for time window $\Delta t = 3.0\,t_\eta$, for the same set of triads as in fig. 4. Top row: PDFs as functions of triad precession frequency and product of triad mode amplitudes. Bottom row: PDFs as functions of triad precession frequency and product of logarithmic time derivative of triad mode amplitudes. Left: $D = 1$. Right: $D = 0.95$.

precession resonances, responsible for perturbations in the energy flux across scales. These resonances occur when the precession frequency $\Omega_{k_1 k_2}^{k_3}$ of a triad phase coincides with a typical nonlinear frequency of the triad's mode amplitudes [22]. Such a search requires the introduction of a *tuning parameter*. Work in this direction will be reported elsewhere.

Another important aspect of this paper consists of the study of the effects produced by the introduction of fractal-Fourier decimation for the 1D Burgers equation. We found clear evidence that decimation drives the system to a loss of temporal and spatial correlations among the surviving triad amplitudes and phases, as figs. 3, 4 and 5 show. In real space, as the dimension D is lowered, the velocity field tends to develop fluctuations in the ramps between shocks. These increasing fluctuations could be linked to the loss of correlation/synchronisation amongst the triad amplitudes and phases. In particular, the significant correlation between triad precession frequencies and amplitude growth in the undecimated case ($D = 1$) is lost as the dimension D is lowered (see fig. 5).

Looking forward, the dynamical systems point of view is worthy of further detailed investigation. We need to understand how phases organise and synchronise during the

dynamical evolution, what is the distribution of critical points in the state space, and how these features change when we reduce the fractal dimension D. In particular, the alternation of trapping events and jumping events experienced by the triad phases in fig. 3 suggests the possibility to develop a model for phase evolution based on a biased random walk with waiting times [31], which in turn could explain the fat tails seen in fig. 4. Finally, we stress that very similar studies can be carried on for the much more complicated case of turbulence in the three-dimensional Navier-Stokes equations. Work in this direction will be reported elsewhere.

References

1. E. Ott, *Chaos in Dynamical Systems* (Cambridge University Press, 1994).
2. M. Cencini, F. Cecconi, M. Vulpiani, *Chaos: From Simple Models to Complex Systems. Series on Advances in Statistical Mechanics*, Vol. **17** (World Scientific, 2010).
3. H.F. Weinberger, *A First Course in Partial Differential Equations With Complex Variables and Transform Methods* (Dover Publications, Inc., 1965).
4. J. Bec, K. Khanin, Phys. Rep. **447**, 1 (2007).
5. Gerald Beresford Whitham *Linear and Nonlinear Waves*, Vol. **42** (John Wiley & Sons, 2011).
6. A.L. Barabási, H.E. Stanley, *Fractal Concepts in Surface Growth* (Cambridge University Press, 1995).
7. E. Hopf, Commun. Pure Appl. Math. **3**, 201 (1950).
8. J.D. Cole, Q. Appl. Math. **9**, 225 (1951).
9. Ya.B. Zeldovich, Astron. Astrophys. **5**, 84 (1970).
10. S.N. Gurbatov, A.I. Saichev, S.F. Shandarin, Month. Not. R. Astron. Soc. **236**, 385 (1989).
11. Z.S. She, E. Aurell, U. Frisch, Commun. Math. Phys. **148**, 623 (1992).
12. M. Vergassola, B. Dubrulle, U. Frisch, A. Noullez, Astron. Astrophys. **289**, 325 (1994).
13. E. Aurell, U. Frisch, A. Noullez, M. Blank, J. Stat. Phys. **88**, 1151 (1997).
14. R. Benzi, L. Biferale, R. Fisher, D.Q. Lamb, F. Toschi, J. Fluid Mech. **653**, 221 (2010).
15. L. Biferale, G. Boffetta, A. Celani, A.S. Lanotte, F. Toschi, Phys. Fluids **17**, 021701 (2005).
16. A.S. Lanotte, L. Biferale, G. Boffetta, F. Toschi, J. Turbul. **14**, 34 (2013).
17. L. Biferale, G. Boffetta, A. Celani, B. Devenish, A. Lanotte, F. Toschi, Phys. Rev. Lett. **93**, 064502 (2004).
18. W. Woyczyski, *Burgers-KPZ Turbulence: Gottingen Lectures* (Springer-Verlag, New York, 1998).
19. M.D. Bustamante, Physica D **240**, 1092 (2011).
20. U. Frisch, *Turbulence: The Legacy of AN Kolmogorov* (Cambridge University Press, 1995).
21. S.B. Pope, *Turbulent Flows* (Cambridge University Press, 2000).
22. M.D. Bustamante, B. Quinn, D. Lucas, Phys. Rev. Lett. **113**, 084502 (2014).
23. M. Buzzicotti, L. Biferale, U. Frisch, S.S. Ray, arXiv: 1601.03697 (2016).
24. R.H. Kraichnan, Phys. Fluids (1958-1988) **10**, 1417 (1967).
25. R.H. Kraichnan, J. Fluid Mech. **47**, 525 (1971).
26. H.A. Rose, P.L. Sulem, J. Phys. (Paris) **39**, 441 (1978).
27. Koji Ohkitani, Shigeo Kida, Physics Fluids A: Fluid Dyn. (1989-1993) **4**, 794 (1992).
28. U. Frisch, A. Pomyalov, I. Procaccia, S.S. Ray, Phys. Rev. Lett. **108**, 074501 (2012).
29. S.S. Ray, Pramana J. Phys. **84**, 395 (2015).
30. A.S. Lanotte, R. Benzi, S. Malapaka, F. Toschi, L. Biferale, Phys Rev. Lett. **115**, 264502 (2015).
31. E.W. Montroll, G.H. Weiss, J. Math. Phys. **6**, 167 (1965).